Nonadiabatic couplings in the collisional removal of $O_2(b\ ^1\Sigma_g^+, v)$ by O_2

F. Dayou,[1,a)] M. I. Hernández,[2] J. Campos-Martínez,[2] and R. Hernández-Lamoneda[3]
[1]*Laboratoire d'Etude du Rayonnement et de la Matière en Astrophysique (UMR 8112 du CNRS), Observatoire de Paris-Meudon, Université Pierre et Marie Curie, Meudon Cedex 92195, France*
[2]*Instituto de Física Fundamental, Consejo Superior de Investigaciones Científicas, Serrano 123, Madrid 28006, Spain*
[3]*Centro de Investigaciones Químicas, Universidad Autónoma del Estado de Morelos, Cuernavaca, Mor. 62210, Mexico*

(Received 3 August 2009; accepted 2 January 2010; published online 28 January 2010)

The effect of nonadiabatic couplings on the collisional removal of $O_2(b\ ^1\Sigma_g^+,v)$ by $O_2(X\ ^3\Sigma_g^-,\ v=0)$ is investigated. Two-dimensional adiabatic and quasidiabatic potential energy surfaces for the excited dimer states and the corresponding nonadiabatic radial couplings have been computed by means of *ab initio* calculations. Alternately, a two-state theoretical model, based on the Landau–Zener and Rosen–Zener–Demkov assumptions, has been employed to derive analytical forms for the nonadiabatic couplings and an adiabatic-to-diabatic transformation only depending on a reduced set of adiabatic energy terms. Compared to the *ab initio* results, the predictions of the model are found to be highly accurate. Quantum dynamics calculations for the removal of the first ten vibrational states of $O_2(b\ ^1\Sigma_g^+,v)$ indicate a clear dominant contribution of the vibration-electronic relaxation mechanism relative to the vibration-translation energy transfer. Although the present reduced-dimensionality model precludes any quantitative comparison with experiments, it is found that the removal probabilities for $v=1-3$ are qualitatively consistent with the experimental observations, once the vibrational structure of the fragments is corrected with spectroscopical terms. Besides, the model served to show how the computation of the adiabatic PESs just at the crossing seam was sufficient to describe the nonadiabatic dynamics related to a given geometrical arrangement. This implies considerable savings in the calculations which will eventually allow for larger accuracy in the *ab initio* calculations as well as higher dimensional treatments. © *2010 American Institute of Physics*. [doi:10.1063/1.3297893]

I. INTRODUCTION

The energy transfer by collisions involving the ground and excited species of molecular oxygen plays a crucial role in the chemistry of the upper Earth's atmosphere. Since they compete with radiative processes, the knowledge of the collisional outcome is needed to understand the observed steady-state populations of molecular oxygen and to properly infer their production efficiencies.[1] In particular, Slanger *et al.*[2] reported the vibrational distribution of the $b\ ^1\Sigma_g^+$ state in the nightglow emission of the atmospheric band system, for vibrational levels up to $v=15$. The distribution is remarkable as it exhibits a bimodal feature, with peaks at $v=3/4$ and $v=12$, and deep minima at $v=1$ and $v=8$. Several experiments[3–5] have been conducted to investigate the collisional removal of $O_2(b\ ^1\Sigma_g^+,\ v=1-3)$ by O_2, which turned out to be the most efficient collider for those vibrational levels.[6] An impressive decrease was found in the removal rate coefficients as v increases from 1 to 3, consistent with the features observed in the vibrational distribution. Among the possible mechanisms responsible of such behavior, the electronic-electronic (E-E) energy exchange process (primes are used to label the identity of the molecules),

$$O_2'(b\ ^1\Sigma_g^+,v) + O_2''(X\ ^3\Sigma_g^-,\ v=0) \rightarrow O_2'(X\ ^3\Sigma_g^-,v) + O_2''(b\ ^1\Sigma_g^+,\ v=0), \quad (1)$$

was thought to be the most likely candidate, based on a consistency between the associated endothermicities and the observed activation energies. However, a detailed theoretical picture of the deactivation process is still missing. Kirillov[7] did give estimations of removal rate coefficients by resorting to the semiclassical Rosen–Zener model[8] but, although the results are consistent with the experimental observations, the formalism rests on the use of empirical parameters and investigation of the underlying nonadiabatic mechanisms was not addressed.

In order to provide a first theoretical insight into the microscopic mechanisms, we investigate in this work the effect of nonadiabatic radial couplings on the collisional removal of $O_2(b\ ^1\Sigma_g^+,v)$ by O_2, by means of *ab initio* methods and quantum dynamics calculations. The removal of vibrational states up to $v=9$ is treated within an isolated two-state model, involving the two electronic states which correlate with the fragments $O_2(b\ ^1\Sigma_g^+)+O_2(X\ ^3\Sigma_g^-)$ of Eq. (1). Although the spin-orbit couplings were found to have dramatic effects on the removal of $O_2(X\ ^3\Sigma_g^-,\ v\geq 25)$ by O_2,[9–11] the radial couplings between the two states of interest are considered here as the main source of nonadiabatic pathways for $O_2(b\ ^1\Sigma_g^+,v)$. The vicinity of the coupling region with re-

a)Author to whom correspondence should be addressed. Electronic mail: fabrice.dayou@obspm.fr.

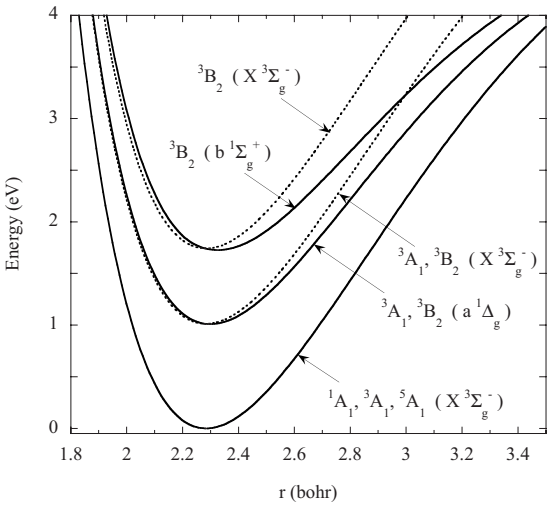

FIG. 1. Low-lying electronic states of the dimer in the $O_2(\alpha,r)+O_2(\beta,r_e)$ asymptotic limit as functions of the active coordinate r and within the C_{2v} point group of symmetry. The states of $O_2(\alpha,r)$ are indicated in parentheses. The two upper curves refer to the states of interest in the present work, $O_2(b\,^1\Sigma_g^+,r)+O_2(X\,^3\Sigma_g^-,r_e)$ (solid line) and $O_2(X\,^3\Sigma_g^-,r)+O_2(b\,^1\Sigma_g^+,r_e)$ (dashed line).

spect to the fragment vibrational states of Eq. (1) provides strong support to the relevance of such a deactivation process, at least for the lowest vibrational states of $O_2(b\,^1\Sigma_g^+,v)$. As shown in the following, the validity of the isolated two-state model is ensured for the entire range of vibrational states studied by the negligible radial couplings found with other states of the dimer unless high interaction energies are sampled.

Given the dimensionality of the system together with the difficulty in dealing with several coupled potential energy surfaces (PESs), we employ a reduced dimensionality model of the dimer. We focus on a particular orientation of the oxygen molecules, the rectangular H orientation,[12] corresponding with the equilibrium geometry of the dimer of D_{2h} symmetry when both molecules are at their equilibrium internuclear distances r_e. Two degrees of freedom are considered, the intermolecular separation R and the internuclear distance r of the vibrationally excited molecule O_2', whereas the vibrationally cold molecule O_2'' is frozen at its equilibrium geometry r_e. By varying the internuclear distance of one of the molecules the system becomes of the C_{2v} symmetry. In Fig. 1 we present a scheme of the low-lying electronic states of the system in the asymptotic limit as functions of the active coordinate r. The two upper curves of the same $^3B_2$ symmetry correspond to the states of interest in the present work, namely, the $3\,^3B_2$ and $4\,^3B_2$ adiabatic states. Due to the near resonance of the latter states around r_e and the noticeable effects of exchange interactions occurring for the chosen H orientation,[13–17] large nonadiabatic radial couplings are expected at finite intermolecular separations.

The reduced dimensionality model considered here cannot yield a quantitative agreement with experimental results, in particular, due to the neglect of the rotational degrees of freedom. Instead, the present study will serve as a necessary step to identify the nonadiabatic mechanisms and to assess their importance in the collision dynamics. The two-dimensional model allows us to investigate the following relaxation pathways of $O_2(b\,^1\Sigma_g^+,v)$:

$$O_2(b,v)+O_2(X,r_e)\rightarrow O_2(b,v')+O_2(X,r_e), \tag{2}$$

$$O_2(b,v)+O_2(X,r_e)\rightarrow O_2(X,v')+O_2(b,r_e), \tag{3}$$

where the $X\,^3\Sigma_g^-$ and $b\,^1\Sigma_g^+$ states are referred to as X and b. The first process is a vibration-translation (V-T) intramolecular energy transfer, and the second one is a vibration-electronic (V-E) intermolecular energy transfer, coincident with the E-E mechanism of Eq. (1) in the case of $v'=v$. The nonadiabatic radial couplings studied here between the $3\,^3B_2$ and $4\,^3B_2$ states are responsible for the V-E relaxation mechanism.

The paper is organized as follows. In Sec. II, after a brief description of the computational methodology, we discuss the results obtained for the *ab initio* PESs and the nonadiabatic coupling matrix elements (NACMEs). In Sec. III, we present a two-state theoretical model providing analytical expressions for the NACMEs and an adiabatic-to-diabatic transformation, and confront them against the results of *ab initio* calculations. Section IV is devoted to the collision dynamics using both *ab initio* and model diabatic PESs. V-E and V-T relaxation mechanisms are investigated and the consistency with the experimental observations is assessed. Conclusions and directions for further investigations are given in Sec. V.

II. *AB INITIO* POTENTIAL ENERGY SURFACES AND NONADIABATIC COUPLINGS

A. Methodology

The two-dimensional $3\,^3B_2$ and $4\,^3B_2$ PESs were obtained from state-average CASSCF calculations, with equal weights for the first four states of the same symmetry. The $2p$ shell of each oxygen atom was included in the active space, leading to 16 electrons distributed among 12 molecular orbitals and to configuration state functions expansions of 28 352 terms. The $5s4p3d2f$ atomic natural orbital basis set[18] was employed throughout the calculations. Within this computational scheme, the PESs were computed for R ranging from 4 to 18 bohr and r from 1.8 to 3.3 bohr. The vibrationally cold molecule O_2'' was held fixed at its equilibrium geometry $r_e=2.28$ bohr. At each point (r,R), quasidiabatic states were generated following a 2×2 adiabatic-to-diabatic transformation $\mathbf{\Psi}^d=\mathbf{U}\mathbf{\Psi}^a$ of the CASSCF wave functions. The unitary transformation matrix $\mathbf{U}$ was determined by maximizing the overlap of both the active orbitals and the configuration coefficients of the wave function expansion with those at a reference geometry,[19] chosen in the present case in the asymptotic limit. Within such a two-state model, the transformation can be written as a function of the mixing angle θ,[20]

$$\begin{pmatrix}\Psi_\alpha^d\\ \Psi_\beta^d\end{pmatrix}=\begin{pmatrix}\cos\theta & \sin\theta\\ -\sin\theta & \cos\theta\end{pmatrix}\begin{pmatrix}\Psi_1^a\\ \Psi_2^a\end{pmatrix}, \tag{4}$$

where the dependence of each quantity on $\mathbf{Q}=(r,R)$ has been omitted for the sake of clarity. The diabatic PESs $V_{\alpha\alpha}^d$ and

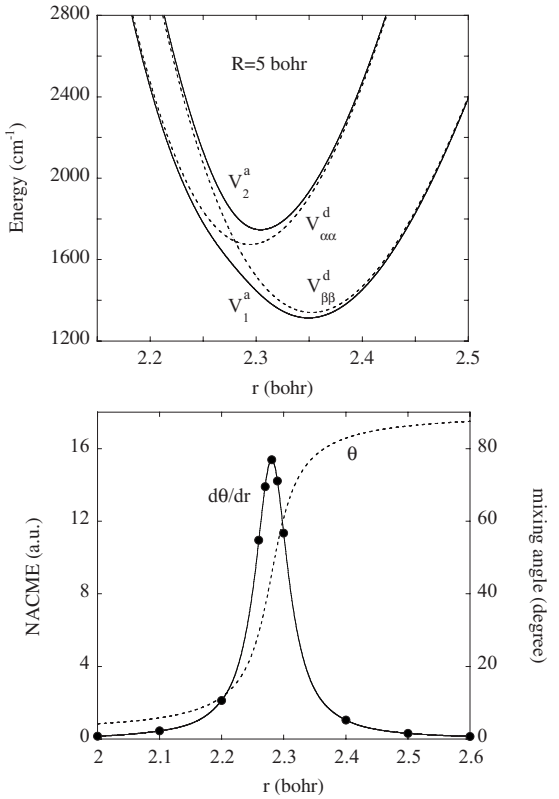

FIG. 2. Upper panel: adiabatic (solid line) and diabatic (dashed line) PESs as functions of the internuclear distance r, for an intermolecular separation of $R=5$ bohr. Lower panel: mixing angle (dashed line) and NACMEs obtained from first derivatives of the mixing angle (solid line) and the finite difference method (full circle).

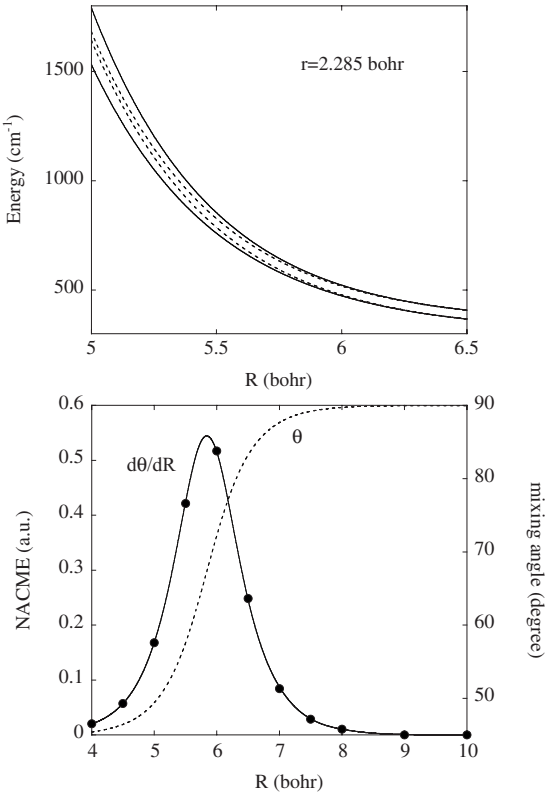

FIG. 3. Same quantities as in Fig. 2, displayed as functions of the intermolecular separation R and for an internuclear distance fixed at $r=2.285$ bohr.

$V_{\beta\beta}^d$ and related coupling $V_{\alpha\beta}^d$ are obtained according to $\mathbf{V}^d=\mathbf{U}^\dagger\mathbf{V}^a\mathbf{U}$. The NACMEs $g_k(\mathbf{Q})=\langle\Psi_1^a|\partial/\partial Q_k|\Psi_2^a\rangle$ have been computed along the two directions as first derivatives of the mixing angle[21,22] $\partial\theta(\mathbf{Q})/\partial Q_k$, with Q_k as the active coordinate r or R. As a check of the diabatization procedure, a three-point finite difference method[23] has been employed to compute the NACMEs at some selected nuclear geometries. Additionally, given the fact that dynamical correlation effects can have a significant influence on the electronic system currently studied, tests calculations were performed at the MRCI level of theory, using the CASSCF wave functions as reference. By freezing the eight core orbitals during the optimization, the MRCI wave functions were comprised of about 18×10^6 contracted configurations (3.5×10^9 uncontracted). The results of MRCI calculations will be discussed in Sec. III C. All *ab initio* calculations have been carried out using the MOLPRO suite of programs.[24]

B. Results

Cuts through the adiabatic $3\ ^3B_2$ and $4\ ^3B_2$ PESs are displayed in Figs. 2 and 3, together with the corresponding diabatic PESs, mixing angle, and NACME. As can be seen, different features are encountered according to the Q_k coordinate being considered. If one looks at the motion along the r direction (Fig. 2), at finite R values, there is an *avoided crossing* between the adiabatic PESs around r_e. Accordingly, the diabatic PESs display a crossing seam along R, centered at $r=r_e$. The mixing angle changes smoothly from 0 to $\pi/2$ along r, consistent with the interchange of electronic character between the adiabatic wave functions as they cross r_e. The NACMEs g_r are bell-shaped functions centered at r_e, of increasing width as R decreases. Along the R direction (Fig. 3), the adiabatic PESs do not display any avoided crossing. Instead, there is an exponentially increasing splitting as we move toward shorter R values. The mixing angle changes smoothly from $\pi/2$ (or 0 if $r<r_e$) to $\pi/4$ as R decreases, consistent with a continuously increasing mixing of states. The resulting diabatic PESs behave as *noncrossing near-resonant* energy curves, and stay almost parallel along R. The NACMEs g_R are again bell-shaped functions. Their width is almost independent of r and their maximum is located where the adiabatic PESs begin to split significantly. Further details regarding particular features of the electronic system will be given in Sec. III.

It can be seen in Figs. 2 and 3 that the NACMEs g_r and g_R derived from the mixing angle are in excellent agreement with those yielded by the finite difference method. A similar agreement has been obtained for all other tested geometries (down to $R=4$ bohr). Such a close agreement between the quantities $\langle\Psi_1^a|\partial/\partial Q_k|\Psi_2^a\rangle$ and $\partial\theta/\partial Q_k$ demonstrates that the residuum couplings $\langle\Psi_\alpha^d|\partial/\partial Q_k|\Psi_\beta^d\rangle$ are negligible along the two directions considered. This is a stringent condition to assess the validity of the 2×2 diabatization procedure.[22] Besides, for most of the intermolecular separations, the calculated mixing angles tend to the proper limiting values (0 and $\pi/2$) such that the adiabatic and diabatic representations coincide when we move far from the avoided crossing region.

This trend is broken for $R \leq 4.5$ bohr and small r, probably due to some contamination of other states not accounted for in the two-state model. In practice, such a contamination has a negligible effect on the calculated transition probabilities, and test calculations showed that the NACMEs between the two pairs of states, ($1\,^3B_2$, $2\,^3B_2$) and ($3\,^3B_2$, $4\,^3B_2$) (see Fig. 1), are quite small down to $R \approx 4$ bohr. In particular, the computed NACMEs between the $2\,^3B_2$ and $3\,^3B_2$ states indicate an inefficient state mixing for the additional avoided crossing which occurs near $r=3$ bohr. We thus have chosen to follow diabatically the states of interest along that crossing region and neglect the related diabatic coupling in the dynamics calculations.

III. FEATURES OF THE $O_2(b\,^1\Sigma_g^+)+O_2(X\,^3\Sigma_g^-)$ SYSTEM AND MODELS OF NONADIABATIC COUPLINGS

The results of the preceding section have shown that an isolated two-state model can be safely employed to describe the nonadiabatic interactions in $O_2(b\,^1\Sigma_g^+)+O_2(X\,^3\Sigma_g^-)$. Within a two-state model, starting from the transformation $\mathbf{V}^a=\mathbf{U}\mathbf{V}^d\mathbf{U}^\dagger$ defined by Eq. (4), the mixing angle writes as

$$\tan(2\theta)=\frac{2V^d_{\alpha\beta}}{V^d_{\beta\beta}-V^d_{\alpha\alpha}}, \tag{5}$$

and, from $g_{Q_k}=\partial\theta/\partial Q_k$, the NACMEs write accordingly[25]

$$g_{Q_k}=\frac{(V^d_{\beta\beta}-V^d_{\alpha\alpha})\frac{\partial}{\partial Q_k}V^d_{\alpha\beta}-V^d_{\alpha\beta}\frac{\partial}{\partial Q_k}(V^d_{\beta\beta}-V^d_{\alpha\alpha})}{(V^d_{\beta\beta}-V^d_{\alpha\alpha})^2+4(V^d_{\alpha\beta})^2}, \tag{6}$$

where the dependence of each quantity on $\mathbf{Q}$ has been omitted for the sake of clarity. In this section, we explore the possibility of obtaining the mixing angle and the NACMEs as functions of the adiabatic energies. This would allow us to construct an adiabatic-to-diabatic transformation using the adiabatic PES as a unique source of information.

A. Features of the $O_2(b\,^1\Sigma_g^+)+O_2(X\,^3\Sigma_g^-)$ system

At $r=r_e$, since the two oxygen molecules are in different electronic states and collide in a symmetrical position with respect to each other, an exchange degeneracy arises.[26,27] The resulting asymptotically resonant $2\,^3B_{3g}$ and $2\,^3B_{2u}$ states show an increasing energy splitting due to exchange interactions[13–16] as the molecules approach each other. The overlap between orbitals of the two diatoms leads to an exponential dependence of the energy splitting with R, as it is found[12,28,29] for the splittings between the dimer spin states dissociating into $O_2(X\,^3\Sigma_g^-)+O_2(X\,^3\Sigma_g^-)$. The breakdown of symmetry induced by the vibrational motion forms states of the same $^3B_2$ symmetry. For r close to r_e, the $3\,^3B_2$ and $4\,^3B_2$ states are asymptotically well approximated by linear combinations of the D_{2h} states, whereas, at short R, they acquire the character of the $2\,^3B_{3g}$ and $2\,^3B_{2u}$ states. It has been previously shown that this feature has noticeable effects on the spin-orbit couplings between the dimer states.[17]

The choice of building the diabatic basis set by requiring a minimum change relative to the asymptotic limit has interesting consequences. Indeed, the resulting diabatic states preserve along R the electronic character which holds asymptotically, i.e., for r close to r_e, the mixture of D_{2h} states. Hence, the diabatic states do not experience any splitting due to exchange interactions, this effect being entirely transferred to the diabatic coupling. Consequently, the diabatic PESs behave as two parallel curves along R, and the diabatic coupling exhibits an exponential dependence with R. Regarding the behavior along r, we found that the energy difference of the diabatic PESs evolves almost linearly with r, whereas the diabatic coupling remains practically constant. The former feature relates to the behavior of the $X\,^3\Sigma_g^-$ and $b\,^1\Sigma_g^+$ diatomic potentials and is verified within a limited range of distances around r_e. The weaker dependence with r of the diabatic coupling $V^d_{\alpha\beta}$ relative to that of $V^d_{\beta\beta}-V^d_{\alpha\alpha}$ is imposed by the condition that $\tan(2\theta)$ must vanish far away from the crossing seam.[30]

B. Models of nonadiabatic couplings

From the features discussed above, we can establish a model for the diabatic matrix elements. We assume that the diabatic coupling is constant along r and equal to its value at the crossing seam,

$$V^d_{\alpha\beta}(\mathbf{Q})=\tfrac{1}{2}\Delta E^a(r_e,R), \tag{7}$$

and the energy difference between the diabatic PESs is constant along R and, hence, equal to its asymptotic value at R_∞,

$$V^d_{\beta\beta}(\mathbf{Q})-V^d_{\alpha\alpha}(\mathbf{Q})=\mp\Delta E^a(r,R_\infty). \tag{8}$$

The sign $\mp$ depends on $r>r_e$ or $r<r_e$, and $\Delta E^a(\mathbf{Q})=V^a_2(\mathbf{Q})-V^a_1(\mathbf{Q})$ is the energy difference between the adiabatic PESs. The mixing angle of Eq. (5) is then given by

$$\theta(\mathbf{Q})=\frac{1}{2}\arctan\left[\mp\frac{\Delta E^a(r_e,R)}{\Delta E^a(r,R_\infty)}\right]+\theta(r,R_\infty), \tag{9}$$

where we imposed the conditions $\theta(r,R_\infty)=\pi/2$ or 0 depending on $r>r_e$ or $r<r_e$, and $\theta(r_e,R_\infty)=\pi/4$. The above equation defines an adiabatic-to-diabatic transformation matrix depending only on the splitting of the adiabatic PESs at the seam and on the splitting between the fragments states.

If one is also interested in obtaining the NACMEs from adiabatic energies, it is convenient to make further assumptions about the behavior of the diabatic matrix elements. In order to represent the NACME along r, Eq. (8) can be reasonably approximated by

$$V^d_{\beta\beta}(\mathbf{Q})-V^d_{\alpha\alpha}(\mathbf{Q})=\Delta s(R_\infty)(r_e-r), \tag{10}$$

where $\Delta s(R_\infty)>0$ is the slope around r_e of the difference between the diatomic potentials. It is worth to note that Eq. (7) together with Eq. (10) correspond to the model originally suggested by Landau[31] and Zener[32] to deal with avoided crossing problems. From Eq. (6), we obtain the well-known Lorentzian shape for g_r,[25,33]

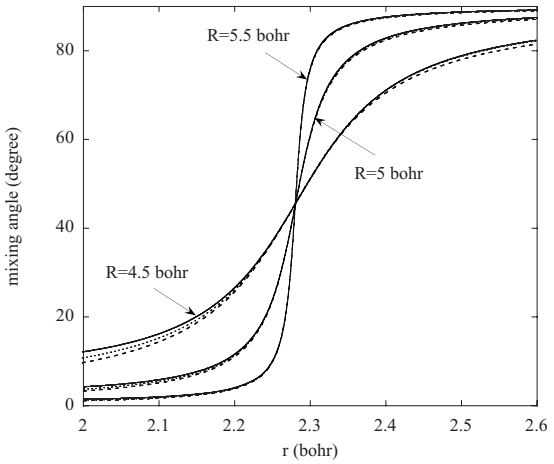

FIG. 4. Mixing angle as a function of the internuclear distance r at selected values of the intermolecular separation R. The results were obtained from the maximal overlap method applied to the CASSCF *ab initio* wave functions (solid line) and the analytical form of Eq. (9), using the *ab initio* values of the relative splitting term $\Delta E^a(r_e,R)/\Delta E^a(r,R_\infty)$ (dashed line) and its approximate form $\pm 2\kappa \exp(-\eta R)/\Delta s(R_\infty)(r-r_e)$ (long dashed line).

$$g_r(\mathbf{Q}) = \frac{1}{2}\frac{\gamma(R)/2}{(r-r_e)^2+[\gamma(R)/2]^2}, \tag{11}$$

where $\gamma(R)=2\Delta E^a(r_e,R)/\Delta s(R_\infty)$. To represent the NACME along R, Eq. (7) can be approximated by

$$V^d_{\alpha\beta}(\mathbf{Q}) = \kappa \exp(-\eta R). \tag{12}$$

Equations (8) and (12) are closely connected to the Rosen–Zener model[8] further extended by Demkov[34] to deal with noncrossing potentials coupled by an exponential interaction function. Accordingly, using Eq. (6), the NACME g_R takes a sec-hyperbolic form,[35]

$$g_R(\mathbf{Q}) = \pm\frac{\eta}{4}\mathrm{sech}(\eta[R-R_M(r)]), \tag{13}$$

where $R_M(r)$ is the value for which g_R has its extremum value,

$$R_M(r) = \frac{-1}{\eta}\ln\left[\frac{\Delta E^a(r,R_\infty)}{2\kappa}\right]. \tag{14}$$

These extrema correspond with the midway points $\theta(r,R_M)-\theta(r,R_\infty)=\pi/8$, where the energy splitting satisfies $\Delta E^a(r,R_M)=\sqrt{2}\Delta E^a(r,R_\infty)$. Details about the two-dimensional mixing angle corresponding to the Landau–Zener and Rosen–Zener–Demkov models are given in the Appendix.

Finally, analytic forms for both g_r and g_R can be derived by taking into account Eqs. (10) and (12) at a time. In this case, the NACMEs write as

$$g_r(\mathbf{Q}) = \frac{1}{2}\frac{1}{a(\mathbf{Q})+[a(\mathbf{Q})]^{-1}}(r-r_e)^{-1}, \tag{15}$$

$$g_R(\mathbf{Q}) = \frac{1}{2}\frac{1}{a(\mathbf{Q})+[a(\mathbf{Q})]^{-1}}\eta, \tag{16}$$

where $a(\mathbf{Q})=2\kappa \exp(-\eta R)/\Delta s(R_\infty)(r-r_e)$ is a particular form of the relative splitting term[36] $\Delta E^a(r_e,R)/\Delta E^a(r,R_\infty)$.

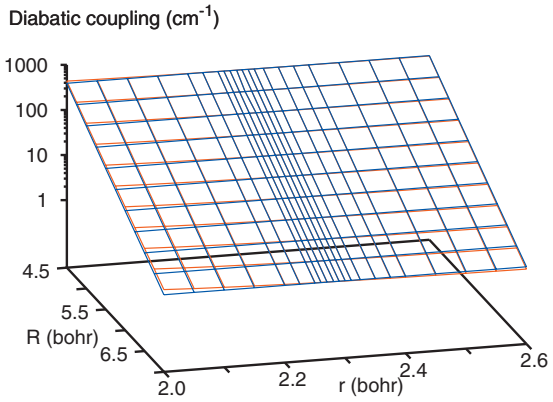

FIG. 5. Diabatic coupling surfaces as functions of the intermolecular separation R and the internuclear distance r. A logarithmic scale is used to highlight the exponential dependence with R of the diabatic couplings. The results were obtained from the adiabatic PESs using the *ab initio* values of the mixing angle (red lines) and the analytical form of Eq. (9) (blue lines), with *ab initio* values of the relative splitting term.

C. Results

We compare in Fig. 4 the mixing angle values yielded by the analytical form of Eq. (9) and the maximal overlap method applied to the CASSCF *ab initio* wave functions (Sec. II A). The analytical mixing angles were derived using both the *ab initio* values of the relative splitting term and its approximate form. In the last case, the parameters κ, η, and $\Delta s(R_\infty)$ were obtained by fitting the *ab initio* splittings $\Delta E^a(r_e,R)$ and $\Delta E^a(r,R_\infty)$ to exponential and linear forms, respectively. As can be seen, the analytical mixing angles present an overall good agreement with the *ab initio* results down to intermolecular separations of about 4.5 bohr. The slightly larger disagreement obtained with the approximate form of the relative splitting term is a direct consequence of the linear dependence imposed for $\Delta E^a(r,R_\infty)$, the exponential dependence of $\Delta E^a(r_e,R)$ being well verified. For $R\leq 4.5$ bohr and small r, the contamination of the wave functions by further states becomes noticeable and breaks down the two-state approximation employed in the modeling. Accordingly, the *ab initio* NACMEs g_r and g_R obtained from the finite difference method (which does not suppose a two-state model) differ by less than 1% with the analytical forms of Eqs. (15) and (16) in the strong coupling regions, except for $R\leq 4.5$ bohr, where discrepancies up to 20% are found. The two-dimensional diabatic coupling $V^d_{\alpha\beta}$ obtained from the analytical adiabatic-to-diabatic transformation applied to the adiabatic PESs is compared in Fig. 5 with the *ab initio* result. As can be seen, both results verify rather well the approximations of the modeling discussed in Sec. III A, i.e., a diabatic coupling constant along r and varying exponentially with R. The agreement between the model and *ab initio* results is quite good around the crossing seam, whereas discrepancies appear for r values distant from the crossing. As will be shown in the next section, these differences, located far from the strong coupling region, have little influence in the nonadiabatic dynamics.

A natural question regarding the accuracy of the present model concerns the dynamical correlation effects, since they can strongly modify the relative position of the two interact-

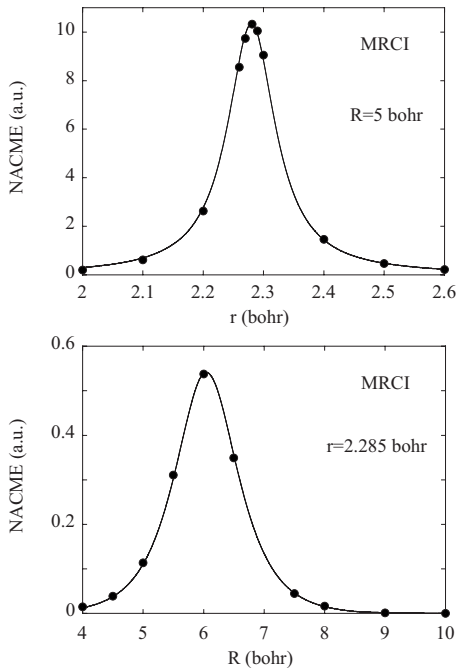

FIG. 6. NACMEs along the internuclear distance r (g_r, upper panel) and along the intermolecular separation R (g_R, lower panel) at selected values of R and r, respectively. The results were obtained from the finite difference method applied to the *ab initio* MRCI wave functions (full circle), and the analytical forms of Eqs. (15) and (16) (solid line).

ing states. We thus performed calculations at the MRCI level of theory (Sec. II A) of the potentials and NACMEs at selected geometries. Compared to the CASSCF results, the MRCI potentials wells are much deeper and displaced toward shorter R, whereas the splitting term $\Delta E^a(r_e,R)$ is significantly larger. Nonetheless, $\Delta E^a(r_e,R)$ was found again very well approximated by an exponential form, and, as can be seen in Fig. 6, the analytical NACMEs g_r and g_R are in excellent agreement with their *ab initio* counterparts. It thus appears that dynamical correlation effects have a significant influence on the PESs, but do not modify the nature of the interaction between the states.

IV. DYNAMICS CALCULATIONS

A. Computational methodology

Within the two-dimensional model, the total Hamiltonian writes $\mathcal{H}=T_R+T_r+H_{\rm el}(\mathbf{q};\mathbf{Q})$, where T_R and T_r are kinetic energy operators associated with the nuclear coordinates $\mathbf{Q}=(r,R)$, $H_{\rm el}$ is the electronic Hamiltonian, and $\mathbf{q}$ collects all the electronic coordinates. The dynamical problem is then readily posed using the diabatic basis set of Eq. (4), whose relevant quantities are the PESs, $V^d_{\alpha\alpha}$ and $V^d_{\beta\beta}$, and the related coupling $V^d_{\alpha\beta}=V^d_{\beta\alpha}$.

The time-independent Schrödinger equation $\mathcal{H}|\Psi^{n_0}\rangle=E|\Psi^{n_0}\rangle$ is solved for each selected initial state n_0 of the diatomic. The total wave function is expanded as

$$\Psi^{n_0}(\mathbf{q},\mathbf{Q})=\sum_{\gamma'=\alpha,\beta}\sum_{v'}^{N(\gamma')} g^{n_0}_{\gamma' v'}(R)\chi_{\gamma' v'}(r)\Psi^d_{\gamma'}(\mathbf{q};\mathbf{Q}), \quad (17)$$

where $N(\gamma')$ is the number of vibrational levels considered for each electronic state $\gamma'=\alpha$ or β, and $\chi_{\gamma' v'}(r)$ are the vibrational wave functions of the diatoms with associated energies $\varepsilon_{\gamma' v'}$. After multiplying by $\langle\chi_{\gamma v}\Psi^d_\gamma|$ and integrating over r and the electronic coordinates, one obtains the set of close-coupled equations,

$$\left[-\frac{\hbar^2}{2\mu}\frac{d^2}{dR^2}-E\right]g^{n_0}_{\gamma v}(R)+\sum_{\gamma' v'}Z_{\gamma v;\gamma' v'}(R)g^{n_0}_{\gamma' v'}(R)=0. \quad (18)$$

The coupling matrix $\mathbf{Z}$ is given by

$$Z_{\gamma v;\gamma' v'}(R)=\varepsilon_{\gamma v}\delta_{vv'}\delta_{\gamma\gamma'} + W_{\gamma v;\gamma v'}(R)\delta_{\gamma\gamma'}+V_{\gamma v;\gamma' v'}(R)(1-\delta_{\gamma\gamma'}), \quad (19)$$

where $W_{\gamma v;\gamma v'}$ are the vibrational couplings within each electronic state,

$$W_{\gamma v;\gamma v'}(R)=\langle\chi_{\gamma v}|V^{\rm int}_{\gamma\gamma}|\chi_{\gamma v'}\rangle, \quad (20)$$

with $V^{\rm int}_{\gamma\gamma}(\mathbf{Q})=V^d_{\gamma\gamma}(\mathbf{Q})-V^d_{\gamma\gamma}(r,R_\infty)$ being the diabatic interaction potential. The vibronic couplings $V_{\gamma v;\gamma' v'}$ are written as

$$V_{\alpha v;\beta v'}(R)=\langle\chi_{\alpha v}|V^d_{\alpha\beta}|\chi_{\beta v'}\rangle. \quad (21)$$

Notice that all couplings vanish asymptotically.

The set of close-coupled equations [Eq. (18)] has been solved by means of the R-matrix propagation method of Light and co-workers.[37,38] The integration range $R=[4,18]$ bohr has been divided into 500 sectors. To get converged results for the removal probabilities up to $v=9$, vibrational bases up to $N(\gamma)=13$ were employed for both $\gamma=\alpha$ and β. The resulting scattering matrix elements $S_{\gamma' v';\gamma v}$ were extracted at the end of the propagation by imposing the usual boundary conditions. The state-to-state probabilities $P_{\gamma v\to\gamma' v'}=|S_{\gamma' v';\gamma v}|^2$ were used to derive the inelastic probabilities, including the V-T relaxation pathway,

$$P^{\rm VT}_{(b,v)}=\sum_{v'\neq v}P_{bv\to bv'}, \quad (22)$$

the V-E relaxation pathway,

$$P^{\rm VE}_{(b,v)}=\sum_{v'}P_{bv\to Xv'}, \quad (23)$$

and the total removal probabilities $P^{\rm tot}_{(b,v)}=P^{\rm VT}_{(b,v)}+P^{\rm VE}_{(b,v)}$. Finally, note that in this approach the two O_2 monomers are treated as distinguishable. A proper treatment of the exchange symmetry should be performed within a full dimensional model including the rotational degrees of freedom.[39,40]

B. Results

In Fig. 7 we report V-T and total inelastic probabilities for the collisional removal of $O_2(b,v=1,3,9)$ by O_2 as functions of kinetic energy. A first set of results corresponds to the diabatic PESs and coupling derived from the *ab initio* mixing angle and CASSCF adiabatic energies reported in Sec. II. A second one corresponds to the probabilities obtained by substituting the mixing angle by the analytic form of Eq. (9), where the approximate form $\pm 2\kappa\exp(-\eta R)/\Delta s(R_\infty)(r-r_e)$ has been used for the relative

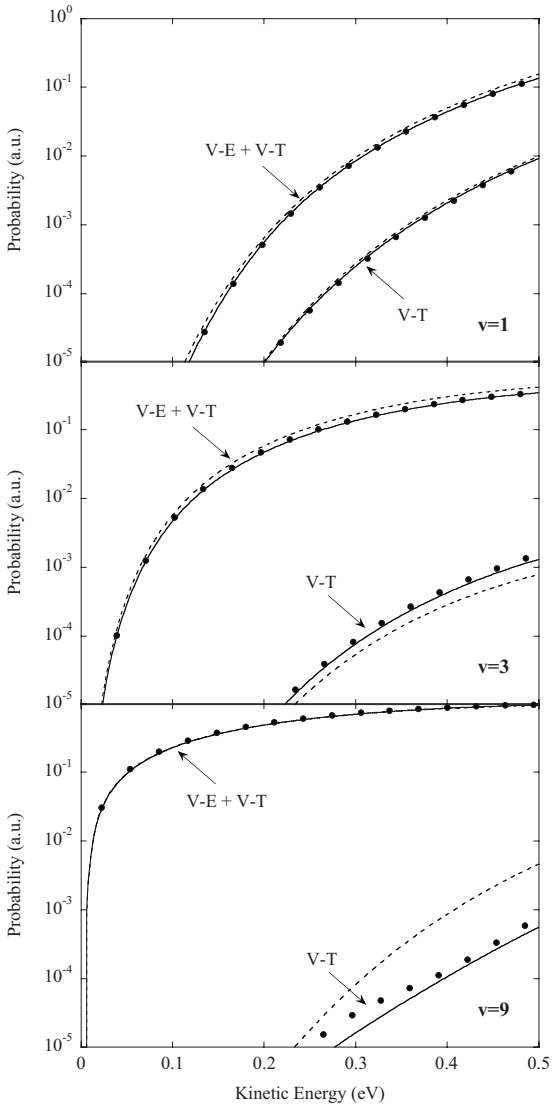

FIG. 7. Inelastic probabilities as functions of kinetic energy for $O_2(b\,^1\Sigma_g^+, v)$ colliding with O_2. The diabatic PESs and coupling considered in the quantum-scattering calculations were derived from adiabatic-to-diabatic transformations constructed from *ab initio* values of the mixing angle (full circles) and the analytic form of Eq. (9) (solid lines). The dashed lines correspond to quantum-scattering calculations where the diabatic interaction potentials and coupling were frozen to its values at the crossing seam. For confrontation with experimental observations, see text and Fig. 8.

splitting term $\Delta E^a(r_e,R)/\Delta E^a(r,R_\infty)$. It is readily seen that the use of the model and *ab initio* diabatic representations provide almost identical results. Only small deviations appear for the probabilities corresponding to the inefficient V-T process, and they are consistent with slight differences observed at short and large values of r between the *ab initio* and model mixing angles (see Fig. 4). A similar agreement is attained for all other vibrational states not shown in Fig. 7. The use of the *ab initio* values of the relative splitting term in Eq. (9) provides only a slight improvement of the small V-T probabilities. The agreement produced by the two-dimensional adiabatic-to-diabatic model transformation, which is constructed solely from knowledge of the relative splitting term, can be considered as remarkable.

We found a strong dependence of the V-E probabilities with the initially selected state v, for the whole range of vibrational states $O_2(b,v=0-9)$ studied. This can be understood in terms of the energy gap law: the largest V-E probabilities occur when the internal energy of a given initial level (b,v) is close to that of an adjacent (X,v') level, i.e., corresponding with a small energy gap $\varepsilon_{bv}-\varepsilon_{Xv'}$. In addition, it has been found that the V-E relaxation mechanism clearly dominates over the V-T energy transfer for all the vibrational levels studied. The preeminence of the V-E energy transfer is the result of favorable energy gaps and of larger vibronic couplings [Eq. (21)], as compared with the $\varepsilon_{bv}-\varepsilon_{bv'}$ energy gaps and the vibrational couplings [Eq. (20)] involved in the V-T process.

As shown in the previous section, the diabatic coupling is practically constant with the vibrational coordinate r and this feature has been already accounted for to build up the model adiabatic-to-diabatic transformation. The preeminence of the V-E process over the V-T one prompted us to test a further approximation, in which both the diabatic interaction potentials and related coupling are fixed at their values along the crossing seam $r=r_e$. Since the mixing angle satisfies $\theta(r_e,R)=\pi/4$, the resulting vibrational and vibronic couplings write

$$W_{\gamma v;\gamma v'}(R) \approx \tfrac{1}{2}[V_1^{a,\mathrm{int}}(r_e,R)+V_2^{a,\mathrm{int}}(r_e,R)]\delta_{vv'}, \tag{24}$$

$$V_{\alpha v;\beta v'}(R) \approx \tfrac{1}{2}\Delta E^a(r_e,R)\langle\chi_{\alpha v}|\chi_{\beta v'}\rangle, \tag{25}$$

where $V_{i=1,2}^{a,\mathrm{int}}(r_e,R)$ are the adiabatic interaction potentials computed along the crossing seam and $\langle\chi_{\alpha v}|\chi_{\beta v'}\rangle$ are overlap integrals between the vibrational wave functions belonging to different electronic states. The resulting removal probabilities are shown in Fig. 7. It can be seen that the total removal probabilities reproduce rather well the results previously obtained, especially in the case of initial levels exhibiting large V-E removal probabilities. This indicates a weak sensitivity of the V-E energy transfer process to the vibrational dependence of the potentials. Furthermore, it is worth noting that the approximate vibrational couplings of Eq. (24) prevent the description of a direct V-T removal process. Despite this, as can be seen in Fig. 7, a qualitative agreement is achieved for the V-T probabilities. This indicates that a sequence of V-E energy transfers must be playing a role in the V-T removal probabilities obtained from the complete calculation.

C. Comparison with experiments

The relevance of the nonadiabatic mechanisms to the removal of $O_2(b,v)$ by O_2 can be assessed by a confrontation with the experimental observations.[3–5] The probabilities of Fig. 7 are not in agreement with observations since they indicate that the removal process becomes more efficient as v increases from one to three quanta, while the opposite behavior is found experimentally.[5] This inconsistency is due to inaccuracies in the *ab initio* set of vibrational energies for the fragments and, specifically, to the neglect of the zero-point energy of the vibrationally cold molecule, whose motion is frozen in the present model. In the following, we replaced the vibrational energies of Eq. (19) by effective values $\varepsilon_{\gamma v}^{\mathrm{eff}}=\varepsilon_{\gamma v}^{\mathrm{RKR}}+\varepsilon_{\gamma' v=0}^{\mathrm{RKR}}$, where $\varepsilon_{\gamma v}^{\mathrm{RKR}}$ are energy levels

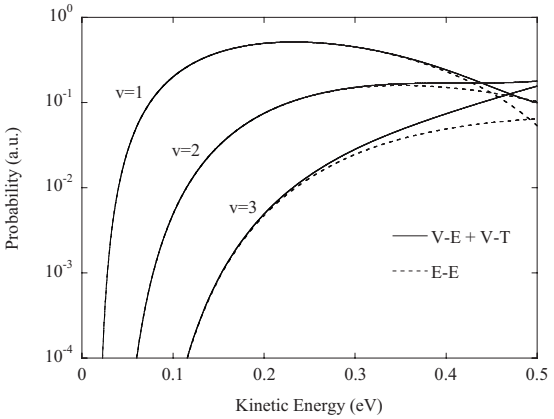

FIG. 8. Inelastic probabilities as functions of kinetic energy for $O_2(b\ ^1\Sigma_g^+,\ v=1-3)$ colliding with O_2, after using spectroscopical terms for the fragments energy levels (see text). Total removal probabilities are shown by solid lines, while dashed lines correspond to the E-E contribution of Eq. (1). After correcting the fragments vibrational structure, the results are now in qualitative agreement with the experiments of Ref. 5.

obtained from accurate Rydberg–Klein–Rees (RKR) potentials[41] of the $O_2(X)$ and $O_2(b)$ diatomic states. The calculations of the removal probabilities have been conducted by resorting to the approximate vibrational and vibronic couplings of Eqs. (24) and (25), using the vibrational wave functions $\chi_{\gamma v}^{\mathrm{RKR}}(r)$ associated with the RKR potentials.

The removal probabilities for $v=1-3$ obtained after correction of the vibrational structure of the fragments are reported in Fig. 8. It can be noticed that the behavior of the probabilities of Fig. 8 is quite different to that of the probabilities of Fig. 7; this shows that using an accurate set of fragment energy levels is crucial, due to the importance of the energy gap law in the energy transfer dynamics. The results of Fig. 8 are now qualitatively consistent with the experiments of Kalogerakis *et al.*,[5] where the measured removal rate coefficients exhibited a strong decrease in the removal efficiency as v goes from 1 to 3 for temperatures between 100 and 300 K (we analyzed the product of present probabilities $P_{b,v}(E_k)$ times $\exp[-E_k/k_BT]$ and found that kinetic energies E_k as high as 0.15 and 0.25 eV for $v=1$ and $v=3$, respectively, are relevant to this function at $T=300$ K). Besides, the activation energies extracted from the near Arrhenius dependence of the removal rate coefficients led Kalogerakis *et al.* to propose that the relaxation mechanism must be dominated by the resonant E-E process [Eq. (1)]. The results shown in Fig. 8 clearly show that the removal of $O_2(b,v)$ at thermal energies proceeds almost completely through the E-E mechanism, in agreement with the expectations of Kalogerakis *et al.* Notice that, due to the distinct vibrational frequencies of the $O_2(X)$ and $O_2(b)$ states, other V-E channels [Eq. (3) with $v' \neq v$] dominate the removal of higher vibrational states. Over the entire range $v=1-9$, we found two maxima in the removal probabilities at $v=1$ and $v=8$, and a minimum at $v=4$. These results provide additional clues for the relevance of nonadiabatic mechanisms in explaining the peaks at $v=3/4$ and deep minima at $v=1$ and $v=8$ observed in the vibrational population distribution of $O_2(b,v)$ in the upper atmosphere.[2]

Similar conclusions can be drawn from the results of Kirillov,[7] who employed the semiclassical Rosen–Zener model[8] with empirical parameters to fit the experimental rate coefficients. We tested the Rosen–Zener formula using the exponential parameter η [Eq. (12)] corresponding to our *ab initio* calculations. The resulting probabilities display a similar trend but quite different values as compared with the quantum probabilities. The interaction might be too strong to satisfy the semiclassical approximation.[36]

V. CONCLUDING REMARKS

The collisional removal of $O_2(b\ ^1\Sigma_g^+,v)$ by O_2 has been studied within a two-degrees-of-freedom model of C_{2v} symmetry, by means of *ab initio* calculations of the relevant PESs and couplings, and quantum dynamics calculations. The calculated removal probabilities indicate that an efficient removal process proceeds through V-E relaxation mechanisms, driven by nonadiabatic radial couplings. After correcting the fragments vibrational structure, the results have been found qualitatively consistent with the experiments of Kalogerakis *et al.*[5] regarding the behavior of the removal probabilities with the initial state selected v and the dominant contribution of resonant E-E processes for $v=1-3$.

The severe reduction in dimensionality in the model precludes any attempt to make a more detailed comparison with the experiments. To achieve a realistic simulation, the full anisotropy of the PESs and couplings should be obtained, and the dynamics should involve all the degrees-of-freedom of the system. In particular, adding the rotational degrees of freedom to the vibronic transitions might play a key role in mitigating the energy gaps and modulating the nonadiabatic couplings. Such a simulation represents a very challenging task, both for the electronic structure as well as for the dynamical part of the computations. Clearly, one should develop a model with the necessary ingredients but making at the same time various reasonable approximations. In this regard, we found here that several approximations reducing considerably the computational effort might be safely applied. First, it has been found that an isolated two-state model is realistic in order to treat the nonadiabatic relaxation dynamics of $O_2(b\ ^1\Sigma_g^+,v)$ up to quite high vibrational levels ($v\approx 9$) and large kinetic energies. Second, analytical forms only depending on the ratio between the splitting of the adiabatic curves along the crossing seam and the difference between the diatomic potentials are found to yield accurate NACMEs and adiabatic-to-diabatic transformation as compared with the *ab initio* results. This avoids costly computations of NACMEs or the use of *ab initio* quasidiabatization procedures, and provides in this way more flexibility in choosing a suitable electronic structure method to describe the system. Besides, the adiabatic energies can be corrected for size consistency, basis set superposition errors, and physical perturbations such as spin-orbit coupling, whereas the usual diabatization procedures do not take into account these issues. Finally, the dominance of the V-E process over the V-T one allowed us to neglect the variation of the diabatic interaction potentials and couplings with the vibrational coordinate.

In summary, the present study indicates that considerable

savings in the theoretical treatment of the title process [or related problems as the collisional removal of $O_2(a\,^1\Delta_g,v)$ by O_2 (Ref. 1)] could be achieved with the computation of two adiabatic PESs just at the crossing seam. Still this is a challenging task since, for a realistic simulation, the effect of the different relative orientations of the oxygen molecules should be included. We found that the couplings are originated from exchange degeneracy effects and symmetry-breaking of the dimer states due to the vibrational motion. Large NACMEs are thus expected for those geometrical arrangements which exhibit a permutation symmetry between the oxygen molecules, such as the H orientation considered here or the linear L geometry,[16] whereas they should be smaller at other geometries. The role of the rotational degrees of freedom in the dynamics should be also taken into account, at least approximately. Moreover, the *ab initio* PESs should include dynamical correlation effects. Test MRCI calculations indicate that the analytical models proposed here also work well at a higher level of theory. Work in these directions is in progress.

ACKNOWLEDGMENTS

Work was partially supported by MEC (Spain, Grant No. CTQ2007-62898-BQU) and by binational CSIC-CONACYT program (Grant No. 2005MX0025/J110.483). The *ab initio* calculations were performed at the IDRIS-CNRS French National Computing Center and on the MPOPM Cluster at the Paris Observatory.

APPENDIX: TWO-DIMENSIONAL MIXING ANGLE WITHIN THE LANDAU-ZENER AND ROSEN-ZENER-DEMKOV MODELS

The NACME g_r corresponding with the avoided-crossing problem takes the Lorentzian form of Eq. (11) when the Landau–Zener assumptions [Eqs. (7) and (10)] are used to model the diabatic matrix elements along the r direction. For the two-dimensional system studied here, this form can be employed to compute the mixing angle along the two directions, through[21,33]

$$\theta(\mathbf{Q}) = \theta(r_0,R_0) + \int_{r_0}^{r} g_r(r',R)dr' + \int_{R_0}^{R} g_R(r_0,R')dR'. \tag{A1}$$

The necessary condition is that there exists a value r_0 of r such that the function $g_R(r_0,R)$ is known. In the present case, we know that $\theta(r_e,R)=\pi/4$, and hence $g_R(r_e,R)=0$. Thus, using $r_0=r_e$ together with Eq. (11), the integral of Eq. (A1) writes

$$\theta(\mathbf{Q}) = \frac{1}{2}\arctan\left[\frac{(r-r_e)}{\gamma(R)/2}\right] + \frac{\pi}{4}. \tag{A2}$$

Similarly, the NACME g_R corresponding with the non-crossing curves problem takes the sec-hyperbolic form of Eq. (13) when the Rosen–Zener–Demkov assumptions [Eqs. (8) and (12)] are used to model the diabatic matrix elements along the R direction. This form can be employed to compute the two-dimensional mixing angle through

$$\theta(\mathbf{Q}) = \theta(r_0,R_0) + \int_{r_0}^{r} g_r(r',R_0)dr' + \int_{R_0}^{R} g_R(r,R')dR', \tag{A3}$$

the necessary condition being that there exists a value R_0 of R such that the function $g_r(r,R_0)$ is known. In the present case, we can use the fact that $g_r(r,R_\infty)=\delta(r-r_e)$ to choose R_0. Then, the integral of Eq. (A3) writes

$$\theta(\mathbf{Q}) = \pm\frac{1}{2}\arctan\left[\tanh\left(\frac{\eta}{2}[R-R_M(r)]\right)\right] \mp \frac{\pi}{8} + \theta(r,R_\infty). \tag{A4}$$

It is worth to note that the forms of Eqs. (A2) and (A4) are fully consistent with those obtained when Eq. (9) is used together with the Landau–Zener and Rosen–Zener–Demkov assumptions.

[1] T. G. Slanger and R. A. Copeland, Chem. Rev. (Washington, D.C.) **103**, 4731 (2003).
[2] T. G. Slanger, P. C. Cosby, D. L. Huestis, and D. E. Osterbrock, J. Geophys. Res. **105**, 20557, doi:10.1029/2000JD900256 (2000).
[3] H. I. Bloemink, R. A. Copeland, and T. G. Slanger, J. Chem. Phys. **109**, 4237 (1998).
[4] E. S. Hwang, A. Bergman, R. A. Copeland, and T. G. Slanger, J. Chem. Phys. **110**, 18 (1999).
[5] K. S. Kalogerakis, R. A. Copeland, and T. G. Slanger, J. Chem. Phys. **116**, 4877 (2002).
[6] L. C. Lee and T. G. Slanger, J. Chem. Phys. **69**, 4053 (1978).
[7] A. S. Kirillov, Adv. Space Res. **33**, 998 (2004).
[8] N. Rosen and C. Zener, Phys. Rev. **40**, 502 (1932).
[9] R. Hernández-Lamoneda and A. Ramírez-Solís, Chem. Phys. Lett. **321**, 191 (2000).
[10] F. Dayou, J. Campos-Martínez, M. I. Hernández, and R. Hernández-Lamoneda, J. Chem. Phys. **120**, 10355 (2004).
[11] F. Dayou, J. Campos-Martínez, M. I. Hernández, and R. Hernández-Lamoneda, J. Chem. Phys. **126**, 194309 (2007).
[12] M. C. van Hemert, P. E. S. Wormer, and A. van der Avoird, Phys. Rev. Lett. **51**, 1167 (1983).
[13] R. Bhandari and L. M. Falicov, J. Phys. C **6**, 479 (1973).
[14] J. Goodman and L. E. Brus, J. Chem. Phys. **67**, 4398 (1977).
[15] B. Bussery and P. E. S. Wormer, J. Chem. Phys. **99**, 1230 (1993).
[16] B. Bussery, Chem. Phys. **184**, 29 (1994).
[17] F. Dayou, M. I. Hernández, J. Campos-Martínez, and R. Hernández-Lamoneda, J. Chem. Phys. **123**, 074311 (2005).
[18] P.-O. Widmark, P.-A. Malmqvist, and B. O. Roos, Theor. Chim. Acta **77**, 291 (1990).
[19] D. Simah, B. Hartke, and H. J. Werner, J. Chem. Phys. **111**, 4523 (1999).
[20] F. T. Smith, Phys. Rev. **179**, 111 (1969).
[21] M. Baer, Chem. Phys. Lett. **35**, 112 (1975).
[22] C. A. Mead and D. G. Truhlar, J. Chem. Phys. **77**, 6090 (1982).
[23] H.-J. Werner, B. Follmeg, and M. H. Alexander, J. Chem. Phys. **89**, 3139 (1988).
[24] MOLPRO, a package of *ab initio* programs designed by H.-J. Werner and P. J. Knowles, Version 2002.6, R. Lindh, F. R. Manby, M. Schütz, *et al.*
[25] M. Oppenheimer, J. Chem. Phys. **57**, 3899 (1972).
[26] G. Herzberg, *Molecular Spectra and Molecular Structure III: Electronic Spectra of Polyatomic Molecules* (Van Nostran Reinhold, New York, 1966).
[27] G. L. Zarur and Y. Chiu, J. Chem. Phys. **56**, 3278 (1972).
[28] R. Hernández-Lamoneda, M. Bartolomei, M. I. Hernández, J. Campos-Martínez, and F. Dayou, J. Phys. Chem. A **109**, 11587 (2005).
[29] M. Bartolomei, M. I. Hernández, J. Campos-Martínez, E. Carmona-Novillo, and R. Hernández-Lamoneda, Phys. Chem. Chem. Phys. **10**, 5374 (2008).
[30] E. E. Nikitin, *Theory of Elementary Atomic and Molecular Processes in Gases* (Oxford University Press, New York, 1974).
[31] L. D. Landau, Phys. Z. Sowjetunion **2**, 46 (1932).
[32] C. Zener, Proc. R. Soc. London, Ser. A **137**, 696 (1932).

[33] M. Desouter-Lecomte, B. Leyh-Nihant, M. T. Praet, and J. C. Lorquet, J. Chem. Phys. **86**, 7025 (1987).
[34] Yu. N. Demkov, Sov. Phys. JETP **18**, 138 (1964).
[35] C. F. Melius and W. A. Goddard III, Phys. Rev. A **10**, 1541 (1974).
[36] E. E. Nikitin, Adv. Quantum Chem. **5**, 135 (1970).
[37] J. C. Light and R. B. Walker, J. Chem. Phys. **65**, 4272 (1976).
[38] E. B. Stechel, R. B. Walker, and J. C. Light, J. Chem. Phys. **69**, 3518 (1978).
[39] A. van der Avoird and G. Brooks, J. Chem. Phys. **87**, 5346 (1987).
[40] J. Pérez-Ríos, M. Bartolomei, J. Campos-Martínez, M. I. Hernández, and R. Hernández-Lamoneda, J. Phys. Chem. A **113**, 14952 (2009).
[41] T. G. Slanger and P. C. Cosby (private communication), 2006.